CDF/PUB/EXOTIC/PUBLIC/7307

Search for the WH Production Using High-p_T Isolated Like-Sign Dilepton Events in Run II

The CDF Collaboration
URL http://www-cdf.fnal.gov
(Dated: October 24, 2004)

We search for the neutral higgs production associated with the W boson using high-p_T isolated like-sign dilepton events in the CDF Run-II data corresponding to an integrated luminosity of 193.5 pb^{-1}. We first study the background components in our base-line like-sign sample which is created by requiring the leading lepton $p_T > 20$ GeV/c and the second lepton $p_T > 6$ GeV/c, and confirm that, overall, the entire sample is consistent with our background expectation. Based on the $S/\sqrt{B}$ calculation using signal Monte Carlo's and our background expectation, the signal region is then determined in the plane of the second lepton p_T (p_{T2}) versus the vector sum of p_T's of the two leptons (p_{T12}). The signal region is $p_{T2} > 16$ (18) GeV/c and $p_{T12} > 35$ GeV/c for the higgs masses < 160 GeV/c^2 (> 160 GeV/c^2). No event is found, while the total background is expected to be 0.95 ± 0.61(stat.) $\pm$ 0.18(syst.) events, the 110 GeV/c^2 bosophilic (fermiophobic) higgs to be about 0.06 events assuming the same production cross section as the Standard Model higgs, and the 160 GeV/c^2 Standard Model higgs to be about 0.03 events. We set cross section upper limits $\sigma(WH) \times B_F(H \rightarrow WW) < 12$ pb at the 95% C.L. for the 110 GeV/c^2 higgs and 8 pb for the 160 GeV/c^2 higgs. This analysis is structured from simple techniques only: conventional isolation, high-p_T lepton identification, and simple kinematical requirements to define the signal region. There is no signal-specific cuts such as missing-E_T and other topological cuts. The present result therefore provides a conservative physics interpretation.

Preliminary Results for Winter 2005 Conferences

I. INTRODUCTION

Our physics objective is to search for the neutral higgs boson using events containing a like-sign dilepton pair as expected in the following reaction:

$$qq' \rightarrow W^{\pm}H \rightarrow W^{\pm}W^{*}W^{*} \rightarrow \ell^{\pm}\ell^{\pm} + X.$$

The relevant higgs mass region is above 160 GeV/c^2 for the Standard Model higgs where the branching fraction of $H \rightarrow W^{*}W^{*}$ supersedes that of $H \rightarrow b\bar{b}$. The search for this signature in the region at low mass is, however, still important because we need to investigate various higgs couplings as an essential test to convince that signals are attributed to the higgs production as we expect. This channel also covers the case beyond the Standard Model that the higgs boson couples only to the gauge bosons, which is referred to as the bosophilic or fermiophobic higgs boson. Such a case is interesting on its own from the view point of experimental physics if we consider the possibility that the mass origins could be different between gauge bosons and fermions. Theoretically, the bosophilic higgs [1] boson appears, for example, in the two higgs doublet model (type I). The production cross section is usually dependent on theoretical parameters such as $\tan\beta$, the ratio between the two vacuum expectation values of the CP-even neutral higgs bosons, but, as a benchmark scenario, we consider it to be the same as the Standard Model in this analysis. The corresponding mass region suitable to our signature is above 110 GeV/c^2 where the branching fraction of $H \rightarrow \gamma\gamma$ is overtaken by this channel. On the experimental side, the like-sign dilepton event is one of the cleanest signature in hadron collisions. This analysis exploiting such a distinctive signature is therefore expected to have a high potential of the sensitivity for the search.

II. DATA SAMPLE & EVENT SELECTION

The data were collected with the CDF II detector [2] between March 2002 and September 2004, corresponding to an integrated luminosity of 193.5 pb^{-1}. The events used in this analysis were selected online with inclusive lepton triggers that require an electron with E_T >18 GeV or a muon with p_T >18 GeV/c. At offline, our approach is to first select high-p_T isolated like-sign events with simple requirements but with enough cleanness, and understand them in terms of backgrounds before any optimization of additional cuts to enhance signal events.

The event vertex with the highest p_T sum of associated tracks is chosen and its z coordinate [3] is required to satisfy $|z_{\rm vtx}| < 60$ cm. The central region ($|\eta| < 1.1$) is considered for the lepton detection, and the leptons are further required to be within fiducial regions of the sub-detectors. We require at least one electron with $E_T > 20$ GeV or muon with $p_T > 20$ GeV/c which is considered to be responsible for firing the corresponding trigger, and at least one other electron with $E_T > 6$ GeV or muon with $p_T > 6$ GeV/c. The leptons are required to be isolated in terms of the calorimeter cone-isolation with a cone size of $R = 0.4$ to be less than 2 GeV, where the isolation is a scaler sum of E_T over calorimeter towers around the lepton, excluding the contribution from the lepton itself, within the range specified by the radius $R = \sqrt{(\Delta\eta)^2 + (\Delta\phi)^2}$ in the η-ϕ space (ϕ is in units of radian). We then apply a series of lepton identification cuts which impose various internal consistencies of information obtained from sub-detectors and require detector responses consistent with electrons or muons. Electron candidates are rejected if an oppositely-charged track consistent with the kinematics of a photon conversion is found.

For the events with two or more leptons that pass our selection above, we apply a cosmic-ray veto, dilepton mass cut ($M_{\ell\ell} > 12$ GeV/c^2), and a Z-decay removal to clean up the sample. We also explicitly require that the leptons must be consistent with coming from the same vertex, which is an important requirement for multi-lepton signatures especially in a high-luminosity situation. The Z removal is implemented aiming mainly to reduce WZ and ZZ backgrounds which are irreducible in our signature. Such a rejection requires efforts to widen the acceptance of leptons from Z decays, since events would seemingly represent like-sign signatures otherwise. For each good lepton candidate, the algorithm therefore looks for in the event an isolated track with oppositely charged or a loosely-identified isolated lepton, including electrons in forward regions, with the same species but without asking charge combination, then rejects the event if the invariant mass falls in a Z mass window between 81 GeV/c^2 to 101 GeV/c^2. The application of Z removal to like-sign lepton pairs, dielectrons particularly, also helps us minimize the contributions originally from opposite-sign pairs with either incorrect charge measurements due to hard bremsstrahlung or charge swaps due to hard photon conversion. We finally require at least one like-sign pair in the event and let the events with three or more leptons remain in our sample.

III. BACKGROUND ESTIMATION

Although the like-sign requirement is quite effective to suppress QCD and known electroweak processes, we expect that fake-lepton backgrounds still remain at a considerable level in the events of our signature. Most of our efforts in background study focus on these fakes.

A. Monte Carlo background samples

We use Monte Carlo samples to estimate a part of backgrounds. They are irreducible diboson backgrounds, WZ and ZZ, and reducible backgrounds such as electroweak processes of Drell-Yan and WW, $t\bar{t}$, and W plus heavy flavor backgrounds. The effective cross sections of the irreducible diboson backgrounds are small due to their small production cross sections and further reductions by the leptonic branching ratios. The reducible QCD and electroweak processes are strongly suppressed by the high-p_T cut, the isolation cut, and the like-sign requirement.

B. Fake lepton background

The physics sources of fake electrons (including non-prompt electrons) are interactive $\pi^{\pm}$, accidental overlap of π^0's and a track, and residual photon conversion, where the residual photon conversion is a single electron originating from the photon conversion with an unobserved partner track due to its low momentum. For the fake muons the sources are punch-through hadron and decay-in-fight muon. Non-interested real leptons from heavy flavors in QCD processes are included here as one type of fake leptons.

We first obtain the fake rate $R_{\rm fake}$ which is defined as the probability for the isolated tracks to pass the lepton selection cuts, then scale, with this rate, the number of isolated like-sign tracks found in addition to the leading (trigger) lepton in the inclusive lepton samples to estimate the fake backgrounds as a lump sum. The isolated track is required to pass $p_T > 6$ GeV/c, the isolation cut, track quality cuts, and a match with the event vertex. The choice of the isolated tracks as the denominator is expected to reduce the sample or the physics-source dependence of the rate. It is not attempted to differentiate the cases that the leading lepton is a fake or real in this analysis.

We evaluate the $R_{\rm fake}$ using inclusive jet samples with $E_T > 20$ GeV (JET20) and $E_T > 50$ GeV (JET50). In this, we require a set of criteria to ensure an unbiased sample of isolated tracks in generic QCD events. The obtained fake rates are shown in Fig. 1 as a function of track p_T. The decrease of the fake-electron rate toward the low-p_T end is due to the E_T cut. We take the average of the fake rates estimated from the two samples as the combined rate and assign a half of the difference as a systematic error due to sample dependence. We also assign a systematic error due to any remaining trigger biases based on studies of the fake rates as a function of azimuthal opening angle between the trigger jet and the isolated track.

We look at the JET100 and inclusive high-E_T (> 25 GeV) photon (not necessarily isolated) samples for validation of the fake lepton rate, where the leptons expected from the fake rate are compared with the observed lepton candidates as shown in Fig. 2. We see reasonable agreements for each sample within the estimated error.

C. Residual photon conversion

The contribution of the residual photon conversion is included in the fake rate as discussed in the previous section. The contribution must be the same between the jet samples and other samples to which the fake rate is applied in order to correctly predict the residual photon conversion background. However, it could be unstable since the photon conversion is a result of complicated physics-processes: π^0 decays to two photons and a succeeding conversion of the photon, thus the probability for the electron (inclusively means the positron as well) from photon conversion to pass our denominator cut defined in the fake rate calculation could change in a different way compared to other fake-components when kinematical biases of samples change. Also the source of photons can be the bremsstrahlung of the electron as well as the decay of π^0 produced in QCD processes. The relative contribution of the production mechanisms therefore could be different depending on the sample. As a check of the stability of the contribution from residual photon conversions, we compare the jet and the inclusive high-p_T lepton samples by means of the photon conversion tagging ratio $R_{\rm conv}$ defined as

$$R_{\rm conv} = \frac{\text{number of photon conversions}}{\text{number of electrons}} \ , \tag{1}$$

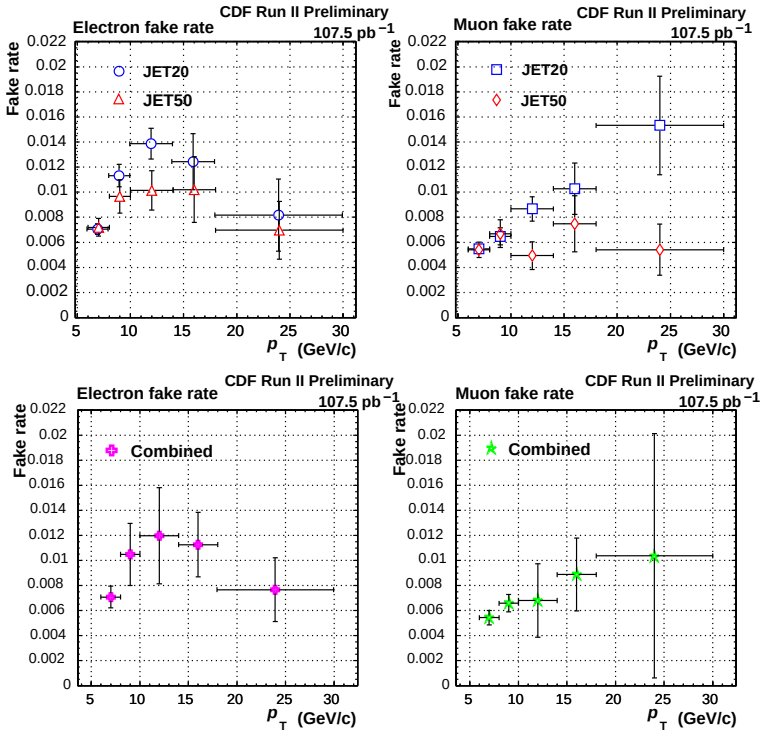

FIG. 1: Track p_T dependence of the fake lepton rate. The upper left (right) plot shows the electron (muon) fake rate for the JET20 and JET50 samples. The lower left (right) plot shows the combined electron (muon) fake rate.

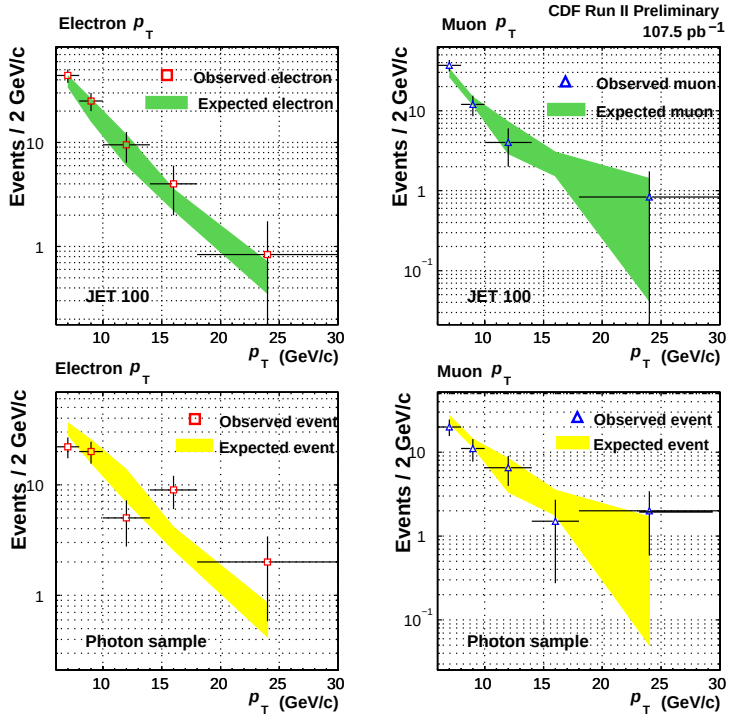

FIG. 2: Expected and observed lepton p_T distributions in the JET100 and high-E_T photon samples. The upper left (right) plot shows the electron (muon) p_T distribution in the JET100 sample. The lower left (right) plot shows the electron (muon) p_T distribution in the high-E_T sample. The filled regions represent the number of expected events with the estimated errors and the points represent the number of observed events.

where the electron in the denominator is the same as our second electron candidates (surviving the photon conversion veto), while the numerator is required to meet the same conditions as the denominator except that the candidates are rather identified as photon conversions. For the inclusive high-p_T lepton samples we collect the like-sign dilepton pairs with the second electron tagged as a photon conversion and compare them to the original like-sign pairs. The photon conversion tagging ratios for two samples of each jet and inclusive lepton category are shown in Fig. 3. Taking the weighted average within each jet and inclusive lepton samples, we obtain $R_{\rm conv} = 0.26 \pm 0.10$ for the jet samples and $R_{\rm conv} = 1.23 \pm 0.26$ for the second electron candidates of like-sign dilepton pairs in the inclusive lepton samples. The observed difference is an evidence that the fraction of the residual photon conversion background is also different between the jet samples and the like-sign dilepton events in the inclusive high-p_T lepton samples. We, hence, try to separate the contribution of residual photon conversions from the fake electron rate. The reason for the observed difference is yet to be understood.

Once we know the total tagging efficiency $\varepsilon_{\rm tot}$, we can estimate the amount of the residual photon conversions from that of the tagged photon conversions by multiplying the residual ratio $R_{\rm res}$ defined as

$$R_{\rm res} = \frac{1-\varepsilon_{\rm tot}}{\varepsilon_{\rm tot}}, \qquad \varepsilon_{\rm tot} = \frac{N_{\rm tag}}{N_{\rm IDele}}, \tag{2}$$

where $N_{\rm tag}$ is the number of tagged photon conversions and $N_{\rm IDele}$ is the number of photon conversions with one leg of electron passing our selection criteria except the photon conversion veto (seed electron). We decompose the photon conversion tagging efficiency into three parts as

$$\varepsilon_{\rm tot} = \varepsilon_{\rm track} \cdot \varepsilon_{\rm cut} \cdot \varepsilon_{\rm pt2.0}, \tag{3}$$

where $\varepsilon_{\rm track}$ is the partner track finding efficiency as a function of p_T with constrained to be fully efficient in the plateau region $p_T > 2$ GeV/c and the dominant source of the inefficiency, $\varepsilon_{\rm cut}$ is the efficiency of the criteria applied to a track pair to identify a photon conversion (tagging cuts), $\varepsilon_{\rm pt2.0}$ is the partner track finding efficiency in the region $p_T > 2$ GeV/c.

We use a Monte Carlo sample to obtain the kinematic information of the photon conversion by generating prompt photons without an assumption of physical process and passing them through the CDF detector simulation program. We parameterize the photon p_T spectrum as ${p_T}^{-\alpha}$, where α is set to 6.9 in order to reproduce the p_T spectrum of electrons from the photon conversion observed in the data. This tuning is necessary because the partner-track p_T is correlated with the seed-electron E_T and we later obtain the efficiency by comparing the partner-track p_T spectra between the data and the Monte Carlo. The flat distribution of the photon density in η and ϕ is used. We check that the energy sharing between the electron and the positron is properly simulated, and that the distribution of conversion point is in a reasonable agreement with the data. Figure 4 shows the p_T spectrum of the partner tracks of the photon conversion for the data and the Monte Carlo. Here the Monte Carlo sample is constrained to match with the data in the region $p_T > 2$ GeV/c where we see little discrepancy. As expected, the track reconstruction is inefficient for low-p_T tracks. The partner track finding efficiency $\varepsilon_{\rm track}(p_T)$ obtained by comparing the data and the Monte Carlo spectra is also included in Fig. 4. It is convenient to express the efficiency as a function of E_T of the seed electron in our analysis, since the seed electron is actually recognized as an electron candidate and the E_T is the canonical parameter for the electron. Thus we redefine $\varepsilon_{\rm track}$ as a function of E_T of the seed electron by convoluting the efficiency function with the p_T spectrum bin-by-by of the E_T, which is presented in Table I.

The remaining other efficiencies in Eq. (3) are measured using a photon conversion sample identified by an independent method from our nominal algorithm. We use the hit information of the central electromagnetic calorimeter and the central electromagnetic strips. The CES (Central Electromagnetic Strips) or Shower Maximum Detector is located at 7 radiation lengths inside the CEM (Central Electromagnetic Calorimeter) and is designed to determine the position as well as the transverse development of the shower. It does that by measuring the charge deposition on orthogonal strips (in the z direction) and wires (in the ϕ direction). A distinct feature of the photon conversion pair is that the electron and the positron have approximately the same z position at any radius. We look for the highest energy CES cluster in the nearest three towers of the wedge next to the seed electron, where the cluster has to be placed in the "right" side ϕ wedge as expected from the charge configuration. We demonstrate that the z position difference dz has a peak around zero in the right side ϕ and does not in the wrong side in Fig. 5, which is obtained from the 8 GeV inclusive electron data.

We measure the efficiencies by counting the number of passed and failed events over the flat distribution of background for dz distributions. Table II lists the tagging cuts efficiencies calculated for several cuts on the electron E_T. By taking the average as the combined value and the standard deviation as the systematic error due to a potential E_T dependence, we obtain

$$\varepsilon_{\rm cut} = 0.921 \pm 0.006\ ({\rm stat}) \pm 0.006\ ({\rm syst})\ . \tag{4}$$

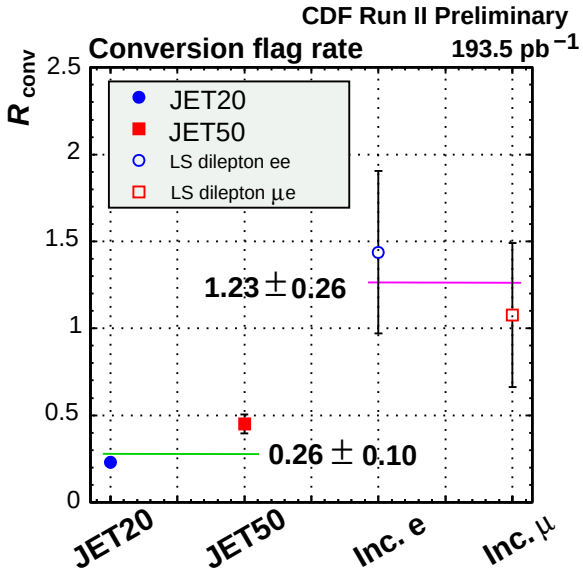

FIG. 3: Photon conversion tagging ratio. A closed circle and a closed square correspond to the jet + electron ($E_T > 6$ GeV) events in the JET20 and JET50 samples, respectively. An open circle and an open square correspond to the second electrons ($E_T > 6$ GeV) of the like-sign ee or μe events in the inclusive high-p_T electron and muon samples, respectively.

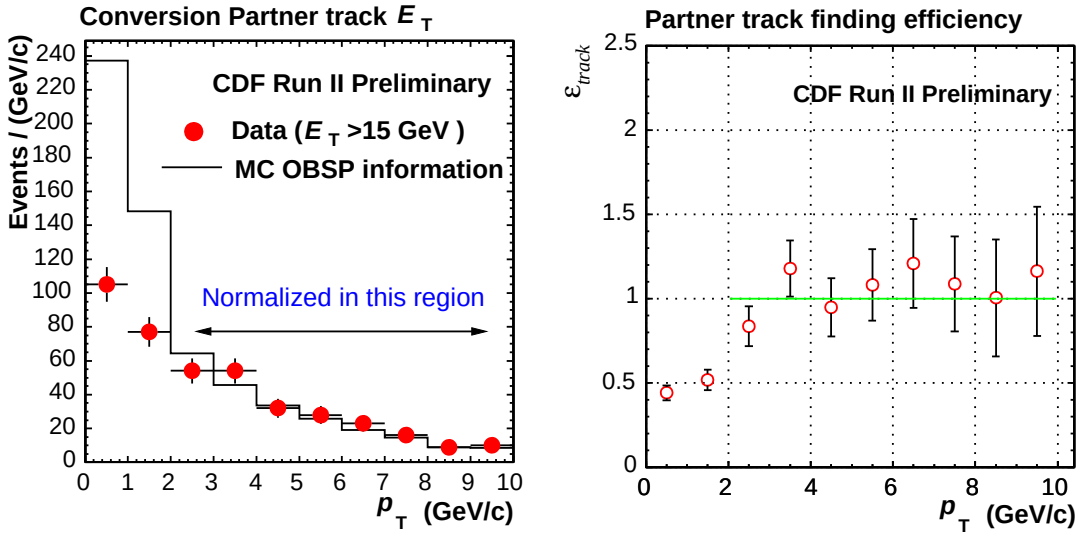

FIG. 4: Partner track p_T spectrum for photon conversions (left). The points correspond to data and the histogram corresponds to the Monte Carlo simulation. The Monte Carlo spectrum is constrained to match with the data in the region of the partner track p_T above 2 GeV/c. The p_T dependence of the partner track finding efficiency (right).

TABLE I: Partner track finding efficiencies for five E_T regions of the photon conversion electrons.

CDF Run II Preliminary

E_T (GeV)	6-8	8-10	10-14	14-18	18-30
$\varepsilon_{\text{track}}$	0.538 ± 0.023	0.567 ± 0.021	0.597 ± 0.020	0.601 ± 0.029	0.686 ± 0.045

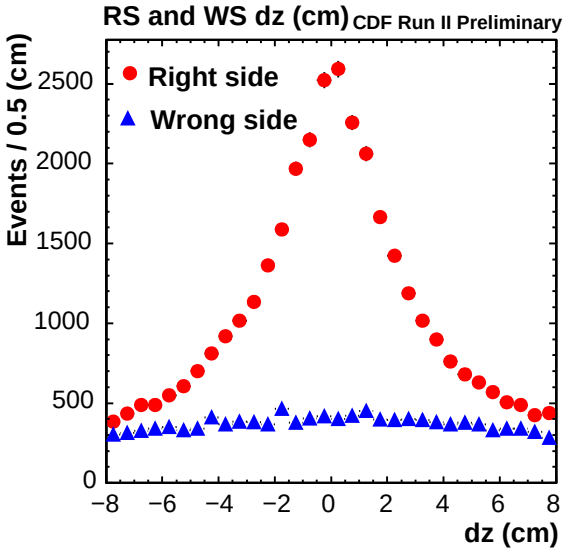

FIG. 5: The z position difference between the electron passing the selection cuts (except the photon conversion veto) and the highest energy CES cluster in the nearest three towers of each ϕ side (right side and wrong side).

TABLE II: Photon conversion tagging cut efficiencies for four E_T cuts on the photon conversion electrons.

CDF Run II Preliminary

E_T (GeV)	> 8	> 10	> 14	> 18
$\varepsilon_{\rm cut}$	0.918 ± 0.003	0.914 ± 0.004	0.926 ± 0.008	0.927 ± 0.010

Similarly, we can measure the track-finding efficiency in the high p_T region (> 2 GeV/c) because the CES method does not rely on the tracking information. In order to ensure the partner track p_T to be greater than 2 GeV/c, we take the following procedure: assume the existence of a track with $p_T = 2$ GeV/c associated with the CES cluster, calculate the track momentum p using the CES z position or η, and require certain energy depositions proportional to the assumed momentum in the CES and the CEM. We then look for the oppositely charged track which is extrapolated to the tower including the CES cluster. The obtained efficiencies are listed in Table III for several cuts on the electron E_T. We take the average as the combined value and the standard deviation as the systematic error due to a potential E_T dependence which could be caused by, for example, contamination of low-momentum tracks with $p_T < 2$ GeV/c. We obtain

$$\varepsilon_{\rm pt2.0} = 0.983 \pm 0.006 \ ({\rm stat}) \pm 0.015 \ ({\rm syst}) \ . \tag{5}$$

We calculate the overall photon conversion tagging efficiency $\varepsilon_{\rm tot}$ defined in Eq. (3) and the residual ratio $R_{\rm res}$ of Eq. (2). The obtained results are shown in Table IV and Fig. 6. We see that $\varepsilon_{\rm tot}$ increases from 50% to 60% as the conversion electron E_T increases.

D. Correction of the electron fake rate

In order to avoid double counting of the residual photon conversion, we make corrections in the original electron fake rate as follows:

$$R_{\rm fake}^{\rm corr} = (1 - R_{\rm conv} \cdot R_{\rm res}) \cdot R_{\rm fake} \ . \tag{6}$$

A technical complication that the $R_{\rm fake}$ is given as a function of track p_T while $R_{\rm res}$ is given as a function of electron E_T is properly taken care of in the correction. The obtained results are shown in Fig. 7, where the original electron fake rates are superimposed for comparison.

TABLE III: Partner track finding efficiencies above 2 GeV/c for four E_T cuts on the photon conversion electrons.

CDF Run II Preliminary

E_T (GeV)	> 8	> 10	> 14	> 18
$\epsilon_{\rm pt2.0}$	0.967 ± 0.005	0.984 ± 0.006	0.996 ± 0.008	0.997 ± 0.006

TABLE IV: Photon conversion tagging efficiencies and residual photon conversion ratios for five E_T regions of the photon conversion electrons.

CDF Run II Preliminary

E_T (GeV)	6-8	8-10	10-14	14-18	18-30
$\varepsilon_{\rm tot}$	0.487 ± 0.046	0.513 ± 0.043	0.540 ± 0.042	0.544 ± 0.057	0.621 ± 0.085
$R_{\rm res}$	1.05 ± 0.19	0.948 ± 0.163	0.856 ± 0.143	0.838 ± 0.191	0.610 ± 0.220

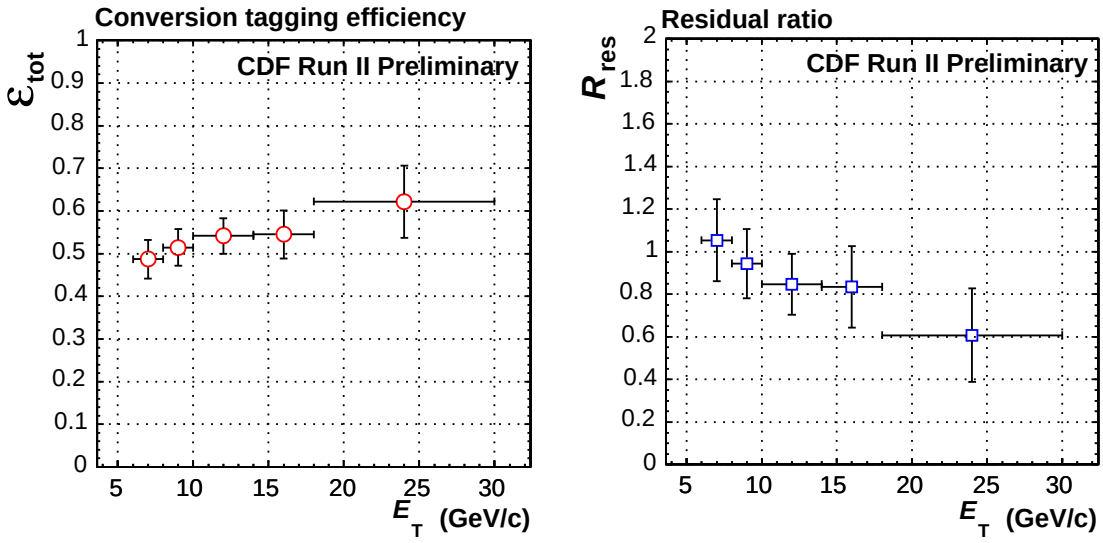

FIG. 6: Electron E_T dependence of the photon conversion tagging efficiency (left) and the residual photon conversion ratio (right).

E. Expected event to data comparison

We compare the expected like-sign dilepton events with the observed ones for the inclusive high-p_T lepton (18 GeV/c), lepton+track (8 GeV/c lepton + 5 GeV/c isolated track), and inclusive low-p_T lepton (8 GeV/c). We look into the second lepton in terms of its transverse momentum p_T, event η, and calorimeter isolation. The comparisons between the expected and observed like-sign dilepton events in the inclusive high-p_T lepton samples are shown in Fig. 8. We sum the like-sign ee, $e\mu$, and $\mu\mu$ events to increase the statistics in the plots. The major background components of the like-sign dilepton events are the fake leptons and the residual photon conversions with the latter being dominant at high-p_T. The contribution of the background estimated by the Monte Carlo simulation is found to be small. We also look into the event topological variables such as $\not\!\!E_T$, lepton-pair azimuthal opening-angle, and vector sum of lepton's p_T for the like-sign dilepton events. The results for the inclusive high-p_T and the lepton+track samples are shown in Fig. 9 and Fig. 10, respectively. The observed number of events in the data is well saturated with our background expectation, and we see reasonable agreements within the statistical errors of the data. Similar agreements are found for the inclusive low-p_T sample. The general agreements also mean that, with the current statistical power of the data, we are not yet sensitive to the sample dependence, if any, of the composition of other fake-lepton components.

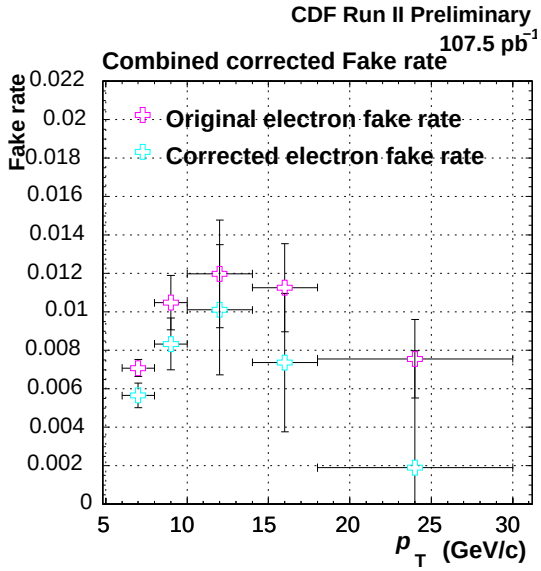

FIG. 7: Original and corrected electron fake-rates. The fake rates are combined values between the JET20 and JET50 samples.

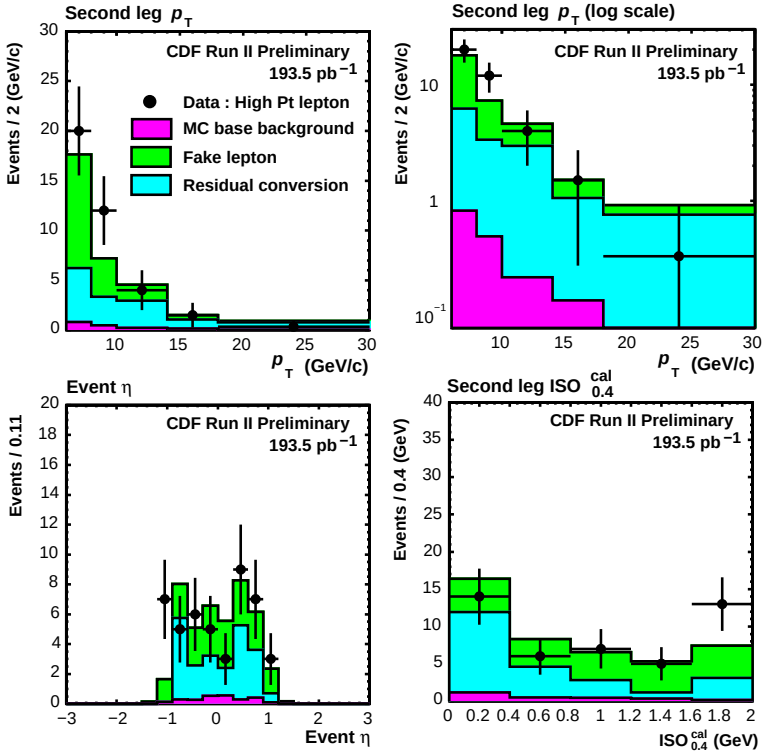

FIG. 8: Expected and observed second lepton p_T in the linear scale (top left) and in the log scale (top right), event η (bottom left), and isolation parameter (bottom right) for the inclusive high-p_T trigger sample.

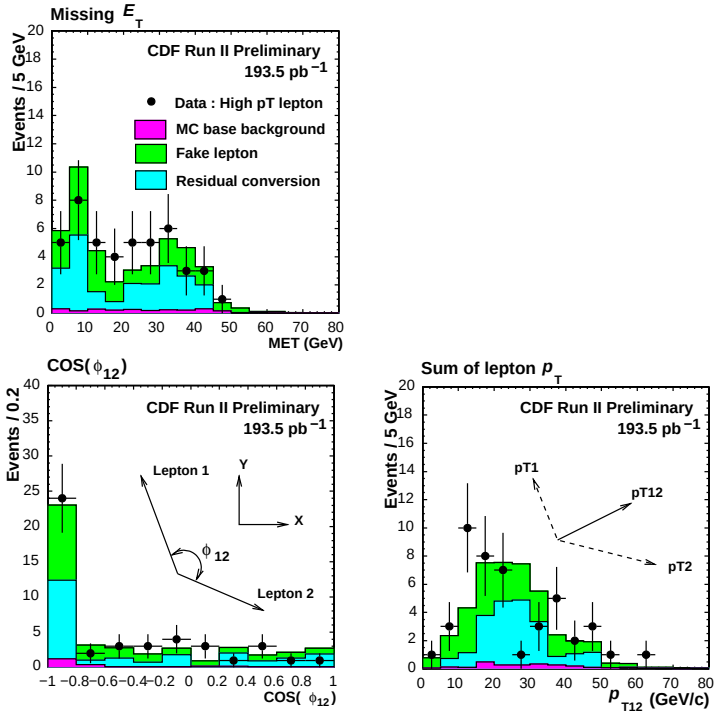

FIG. 9: Expected and observed missing transverse E_T (top left), lepton-pair azimuthal opening angle (bottom left), and vector sum of p_T's of the two leptons $p_{\mathrm{T}12}$ (bottom right) for the like-sign dilepton events in the inclusive high-p_T trigger sample.

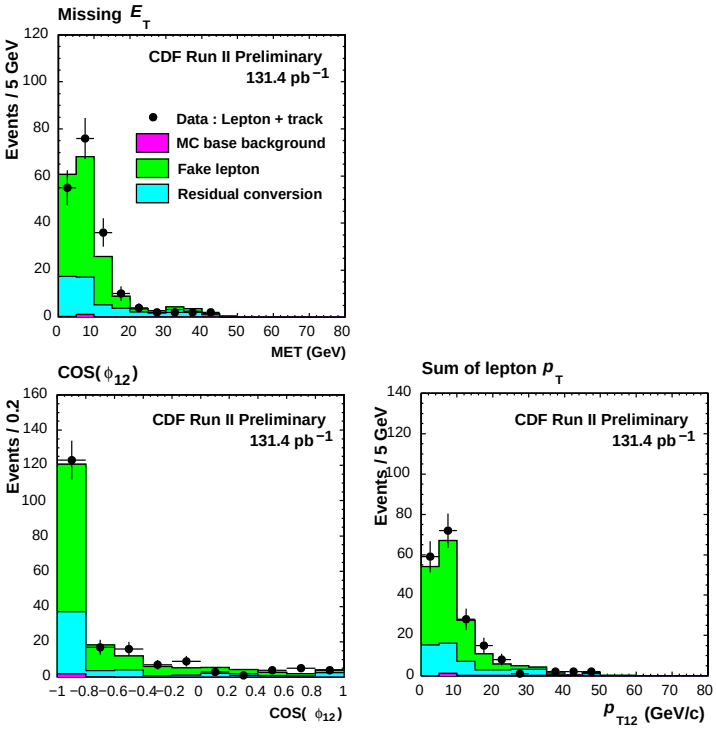

FIG. 10: Expected and observed missing transverse E_T (top left), lepton-pair azimuthal opening angle (bottom left), and vector sum of p_T's of the two leptons $p_{\mathrm{T}12}$ (bottom right) for the like-sign dilepton events in the lepton+track data.

IV. SIGNAL REGION

We determine a signal region in the plane of the second lepton p_T (p_{T2}) and the vector sum of p_T's of the two leptons (p_{T12}) to enhance the signal significance. We use 110 GeV/c^2 bosophilic higgs and 160 GeV/c^2 Standard Model higgs Monte Carlo events as signal samples and the total number of expected backgrounds, then look for the region to improve the signal significance ($S/\sqrt{B}$) as much as reasonable to the extent that we can expect at least about one signal-event with the base-projection of the integrated luminosity in Run II which is 4.4 fb^{-1}. The cut, referred to as the "topological" cut in this analysis, is chosen to be (p_{T2}, p_{T12}) = (16, 35) GeV/c for the higgs mass less than 160 GeV/c^2 and (18, 35) GeV/c for the higgs mass equal or more than 160 GeV/c^2. The number of expected events is 1.5 for the 110 GeV/c^2 case and 0.74 for the 160 GeV/c^2 case. We note that this discussion is not representing a true optimization since the result is subject to the statistical fluctuation of the sample used to derive the background expectations. We therefore look at only the trend of the significance change with different cut values. Our choice of the signal region is rather connected to the fact that we would observe one event on the average in the full data of 4.4 fb^{-1}.

We divide the p_{T2} versus p_{T12} plane into four regions: A, B, C, and the signal region. We compare the number of expected background events with that of observed ones in the control regions (A–C) as a sanity test. Table V shows the result of comparison. Table VI shows the signal events, the breakdown of backgrounds, and observed events in the signal region. The statistical errors of the total background estimates reflect the Monte Carlo statistics and the sample statistics to which the fake rate and the residual photon conversion ratio are applied, while the systematic errors originate from the error of the fake rate and the residual photon conversion ratio. Figure 11 shows the observed p_{T2} versus p_{T12} scatter plot. The major background components in the region A and the signal region are the residual photon conversion, while the fake lepton and the residual photon conversion dominate in the other regions. In each control region we see a reasonable agreement, while we observe no event in the signal region.

V. SIGNAL EFFICIENCY

The total detection efficiency is decomposed into several factors as

$$\varepsilon_{\rm tot} = A \cdot \varepsilon_{\rm iso} \cdot \varepsilon_{\rm ID} \cdot \varepsilon_{\rm dil} \cdot \varepsilon_{\rm topo} \cdot \varepsilon_{\rm trig} \ , \tag{7}$$

where A is the geometrical and kinematical acceptance, $\varepsilon_{\rm iso}$ is the isolation cut efficiency, $\varepsilon_{\rm ID}$ is the lepton identification efficiency, $\varepsilon_{\rm dil}$ is the dilepton selection efficiency, $\varepsilon_{\rm topo}$ is the topological efficiency, and $\varepsilon_{\rm trig}$ is the trigger efficiency. The order of multiplication has a meaning and we calculate the efficiencies sequentially. The signal Monte Carlo samples are generated by PYTHIA of version 6.2 [4]. The process of our interest is $WH \rightarrow WW^*W^* \rightarrow$ dilepton or trilepton (≥ 2 leptons), where the lepton is electron or muon only. The branching ratio of WW^*W^* into ≥ 2 leptons is $\simeq 12\%$. We quote the efficiency with respect to this initial ≥ 2-lepton events. Where it is possible, we introduce scale factors to correct for discrepancies of the efficiencies between the data and the Monte Carlo samples by using well-defined events such as $Z \rightarrow ee$ and $\mu\mu$, then apply those factors to the signal Monte Carlo. The total efficiencies for various higgs masses are shown in Fig. 12. The efficiency varies from 1% at the low-mass region to 1.5% at the high-mass region. The mass dependence of the efficiency is mainly due to a strong mass-dependence of the p_T distribution of the second lepton.

We also look at the efficiency when we expand the analysis to include the process involving the Z boson instead of the W boson ($VH \rightarrow VV^*V^*$), and find it to be about 1% at the high-mass region. The improvement is minimal because the Z removal rejects newly included events. We need a different approach to improve the sensitivity to the higgs production by including events containing the Z bosons.

VI. SYSTEMATIC UNCERTAINTIES

The systematic errors of the background estimation are described in III. We list the sources of systematic error related to the signal efficiency in Table VII. We use the 160 GeV/c^2 higgs sample as the reference. The statistical uncertainty of the Monte Carlo sample is about 4%. We also investigate the variation of the acceptance due to the uncertainties in the parton-density function (PDF), the initial-state radiation (ISR), and the final-state radiation (FSR). The total systematic error is 6.4%. To check the mass dependence we make 110 GeV/c^2 higgs-mass samples and find the total systematic error to be 7.4%. The mass dependence of the systematic error is not large.

TABLE V: Expected background events and observed events in the control regions.

CDF Run II Preliminary (193.5 pb^{-1})

Region	Expected event	Observed event
A	6.2 ± 2.0(stat) ± 1.4(syst)	3
B	29.3 ± 3.8(stat) ± 3.3(syst)	30
C	8.1 ± 2.1(stat) ± 1.0(syst)	12
A+B+C	43.6 ± 3.3(stat) ± 5.1(syst)	45

TABLE VI: Expected signal events, breakdown of background components, and observed events in the signal region.

CDF Run II Preliminary (193.5 pb^{-1})

Process	Expected events (± stat)
Bosophilic $WH(110)$	0.056 ± 0.004
SM $WH(160)$	0.034 ± 0.002
WZ	0.14 ± 0.09
ZZ	0.013 ± 0.010
$t\bar{t}$	0.0097 ± 0.0075
$WQ\bar{Q}$	0.0033 ± 0.0032
WW	0.0034 ± 0.0033
Z/γ^*	0.051 ± 0.037
Fake Lep.	0.12 ± 0.01
Residual photon conversion	0.61 ± 0.61
Total	0.95 ± 0.61(stat) ± 0.18(syst)
Observed event	0

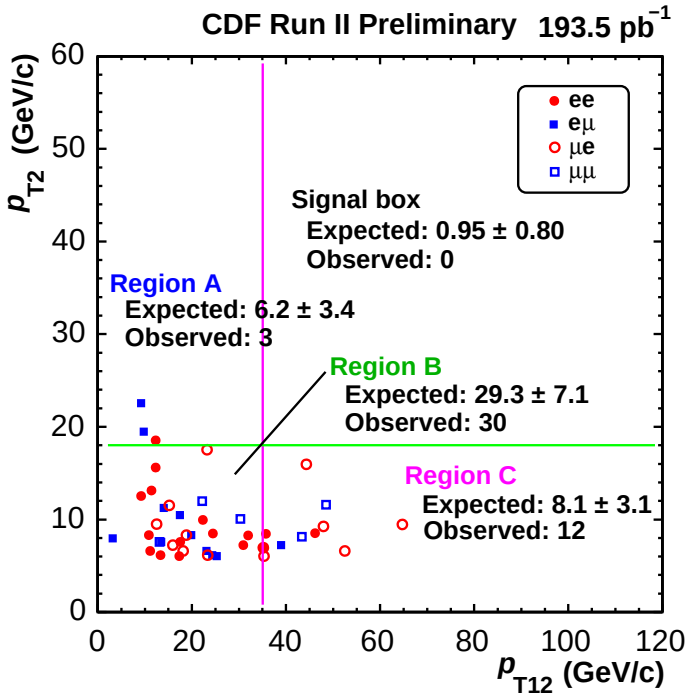

FIG. 11: The p_{T2} vs. p_{T12} scatter plot for the like-sign dilepton events in the inclusive high-p_T lepton samples.

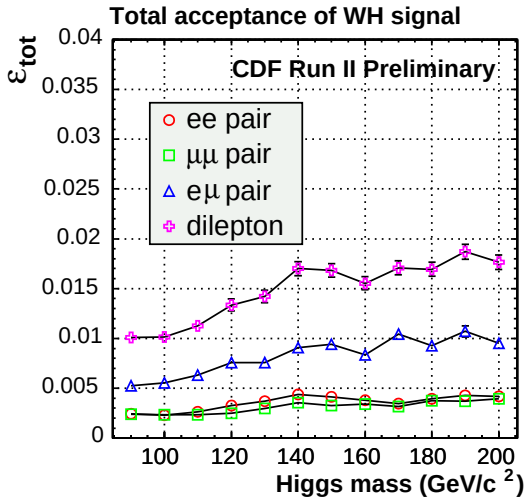

FIG. 12: Total signal efficiency as a function of higgs mass for the WH production. It is defined relative to the total $\geq$ 2-lepton events produced in $WH \rightarrow WW^*W^*$. The circle is dielectron, the square is dimuon, the triangle is $e\mu$, and cross is the dilepton total (including trilepton events).

TABLE VII: Systematic errors of the efficiency.

Higgs mass = 160 GeV/c^2 CDF Run II Preliminary

Sources	ee (%)	$\mu\mu$ (%)	$e\mu$ (%)	Dilepton (%)
Uncertainties of lepton ISO and ID scale factors	0.20	0.15	0.28	0.37
Uncertainties of trigger efficiencies	1.8	0.11	1.6	2.4
Statistical uncertainties of the MC	1.7	1.5	2.4	3.7
Uncertainties from PDF's	1.1	1.6	1.6	1.5
Difference of FSR	4.8	4.3	1.8	3.2
Difference of ISR	2.8	3.5	2.9	3.0
Total (160 GeV/c^2)				6.4
Total (110 GeV/c^2)				7.5

VII. RESULTS

Given that we observe no event in the signal region, we set upper limits on $\sigma(WH) \times B_F(H \rightarrow WW)$ in the Bayesian framework. The result is shown in Fig. 13. We find that the limit is 12 pb at the 95% C.L. for the higgs mass 110 GeV/c^2 and 8 pb for the higgs mass of 160 GeV/c^2.

VIII. CONCLUSIONS

We searched for the neutral higgs boson using high-p_T isolated like-sign dilepton events in CDF Run-II data corresponding to an integrated luminosity of 193.5 fb^{-1}. We observed no event in the signal region of the second lepton p_T greater than 16 GeV/c and the vector sum of p_T's of the two leptons greater than 35 GeV/c. The upper limit on the production cross section times the branching fraction, $\sigma(WH) \times B_F(H \rightarrow WW)$, was obtained to be 12 pb at the 95% C.L. for the higgs mass of 110 GeV/c^2 and 8 pb for 160 GeV/c^2. The analysis is essentially based on only the high-p_T isolated like-sign signature without further introducing signal-specific cuts. The result is thus conservative for the higgs search, while the fact that we observed no event is easily applied to various search analyses. Gven that we looked at the data with an integrated luminosity of about 200 pb^{-1}, the same fact also confirms that the like-sign dilepton signature is very clean in hadron collisions. The signal event yields show that improvements of the efficiency are certainly necessary. In this context, the signal-to-background ratios of 1/20–1/30 already obtained in this analysis without performing detailed optimization of more signal-specific cuts indicate that the sensitivity of this signature to the higgs production is potentially high.

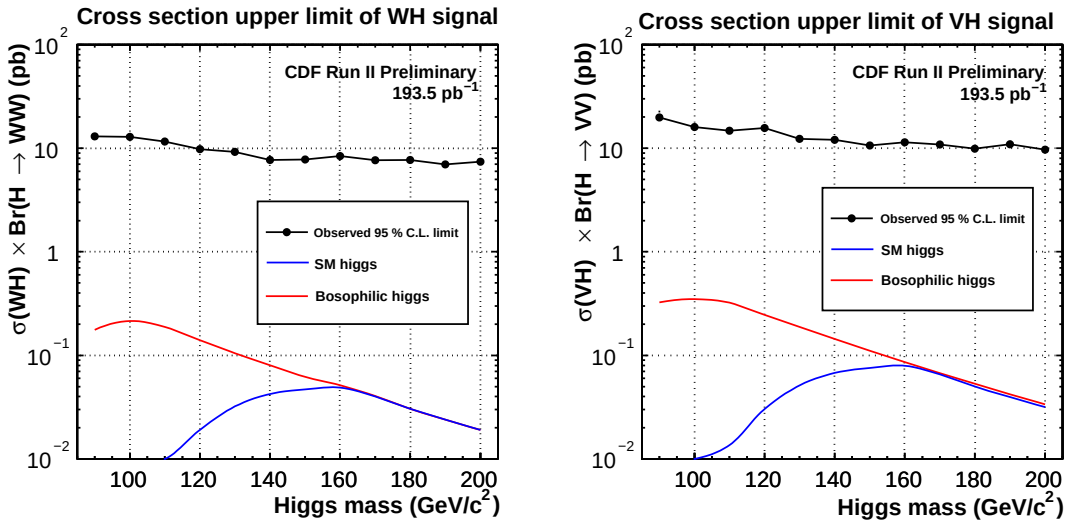

FIG. 13: Left (Right) plot shows 95% C.L. upper limits on the production cross section times branching fraction as a function of higgs mass for the WH (VH) production, together with the cross sections of the Standard Model and of the benchmark scenario for the bosophilic higgs.

Acknowledgments

We thank the Fermilab staff and the technical staffs of the participating institutions for their vital contributions. This work was supported by the U.S. Department of Energy and National Science Foundation; the Italian Istituto Nazionale di Fisica Nucleare; the Ministry of Education, Culture, Sports, Science and Technology of Japan; the Natural Sciences and Engineering Research Council of Canada; the National Science Council of the Republic of China; the Swiss National Science Foundation; the A.P. Sloan Foundation; the Bundesministerium fuer Bildung und Forschung, Germany; the Korean Science and Engineering Foundation and the Korean Research Foundation; the Particle Physics and Astronomy Research Council and the Royal Society, UK; the Russian Foundation for Basic Research; the Comision Interministerial de Ciencia y Tecnologia, Spain; and in part by the European Community's Human Potential Programme under contract HPRN-CT-20002, Probe for New Physics.

[1] A. Stange, W.Marciano, and S.Willenbrock, Phys. Rev. D49 1354 (1994).

[2] F. Abe *et al.*, Nucl. Instrum. Methods Phys. Res. Sect. A **271**, 387 (1988); D. Amidei *et al.*, Nucl. Instum. Methods Phys. Res. Sect. A **350**, 73 (1994); F. Abe *et al.*, Phys. Rev. D **52**, 4784 (1995); P. Azzi *et al.*, Nucl. Instrum. Methods Phys. Res. Sect. A **360**, 137 (1995); The CDF collaboration, "The CDF II Detector Technical Design Report", Fermilab-Pub-96/390-E (1996).

[3] In the CDF coordinate system, θ is the polar angle with respect to the proton beam direction and ϕ is the azimuthal angle. The pseudorapidity is defined as $-\ln(\tan(\theta/2))$. The transverse momentum of a particle is $p_T = p\sin\theta$. The transverse energy defined for calorimeter responses is similarly given by $E_T = E\sin\theta$. The missing transverse energy $\not\!\!E_T$ is the vector pointing opposite the vector sum of transverse energies over all the calorimeter towers.

[4] T. Sjostrand, L. Lonnblad, and S. Mrenna, Comput. Phys. Commun. **135**, 238 (2001).